Earth-like worlds on eccentric orbits: excursions beyond the habitable zone

Darren M. Williams[1] and David Pollard[2]

[1]*Penn State Erie, The Behrend College, School of Science, Station Road, Erie, PA 16563-0203, USA*
e-mail: dmw145@psu.edu
[2]*Earth System Science Center, The Pennsylvania State University, University Park, PA 16802, USA*
e-mail: pollard@essc.psu.edu

Abstract: Many of the recently discovered extrasolar giant planets move around their stars on highly eccentric orbits, and some with $e \geqslant 0.7$. Systems with planets within or near the habitable zone (HZ) will possibly harbour life on terrestrial-type moons if the seasonal temperature extremes resulting from the large orbital eccentricities of the planets are not too severe. Here we use a three-dimensional general-circulation climate model and a one-dimensional energy-balance model to examine the climates of either bound or isolated earths on extremely elliptical orbits near the HZ. While such worlds are susceptible to large variations in surface temperature, long-term climate stability depends primarily on the average stellar flux received over an entire orbit, not the length of the time spent within the HZ.

Received 26 September 2001

Key words: eccentric orbits, extrasolar planets, habitable zone and planetary climate.

Introduction

The number of planetary objects known to orbit nearby stars is now 75, and the list of detections continues to outpace theoretical explanation. The smallest object that has been discovered by radial-velocity surveys thus far has a minimum mass $m \sin i = 0.16 M_J$, or ~ 0.6 times the mass of Saturn, and the range of orbital radii, or semi-major axes, is $0.038 < a < 3.47$ AU (Fig. 1 and Table 1). The parent stars range in spectral type from F7 to M5, with 53 stars being earlier than K0, and all are luminosity class IV or V. This means that all of the stars with planets are either still in their hydrogen-burning phase of stellar evolution on the main sequence, or they are just leaving it. Although the stars are generally similar to the Sun, they are truly quite different from one another with absolute luminosities ranging from $0.0191 L_\odot$ (M5V star GL876) to $56.12 L_\odot$ (K 2III star HIP75458). Here stellar luminosity L is estimated from the apparent bolometric magnitude of a star, which is related to the apparent visual magnitude V through the equation

$$m_{\mathrm{bol}_*} = V + BC,$$

where BC is the theoretical bolometric correction (tables A13 and 14 of Carroll & Ostlie 1996). The V magnitudes and the semi-annual parallactic shifts p for the stars were obtained from the on-line Hipparcos catalogue (see references), which yielded stellar distances $(d = 1/p)$ and luminosities though the equation

$$\left(\frac{L_*}{L_\odot} \right) = \left(\frac{d_*}{d_\odot} \right)^2 10^{(m_{\mathrm{bol}_*} - m_{\mathrm{bol}_\odot})/2.5}, \tag{1}$$

where $d_\odot = 1$ AU $= 4.84 \times 10^{-6}$ pc and $m_{\mathrm{bol}_\odot} = -26.82$. Obtaining accurate stellar data is important because it is luminosity along with star–planet separation that most strongly affects whether a terrestrial world might harbour water-dependent life.

Classically, the spherical region around a star in which a terrestrial body receives an amount of starlight appropriate for sustaining liquid water on its surface at a specific moment in time is called the habitable zone, or HZ. Stars brighten as they evolve so the HZ expands over time. If stars do not evolve too rapidly, a planet like Earth might be able to stay within the HZ boundaries for billions of years. The region of space in which a world would be able to sustain liquid water on its surface for billion-year time-scales is called the continuously habitable zone, or CHZ. Because the simplest life forms on Earth did not require billions of years to evolve, terrestrial planets (or terrestrial moons of giant planets (Williams *et al*. 1997)) within either the CHZ or wider HZ around a Sun-like star will be prime targets for astrobiological research.

The exact boundaries of circumstellar HZs vary slightly from system to system because planets have different volatile inventories and masses, which affect the rate of atmospheric escape of water near the inner edge and the rate of global refrigeration near the outer edge. The limits often quoted today are those of Kasting and colleagues (Kasting *et al*. 1993) who used a radiative–convective climate model to examine the fate of Earth were it slightly closer to or further from the Sun than it is today. The inner edge of the current HZ around the Sun lies between 0.95 AU, where the Earth's stratosphere would become moist (the present stratosphere is kept dry by a steep atmospheric lapse rate, which causes most of the water
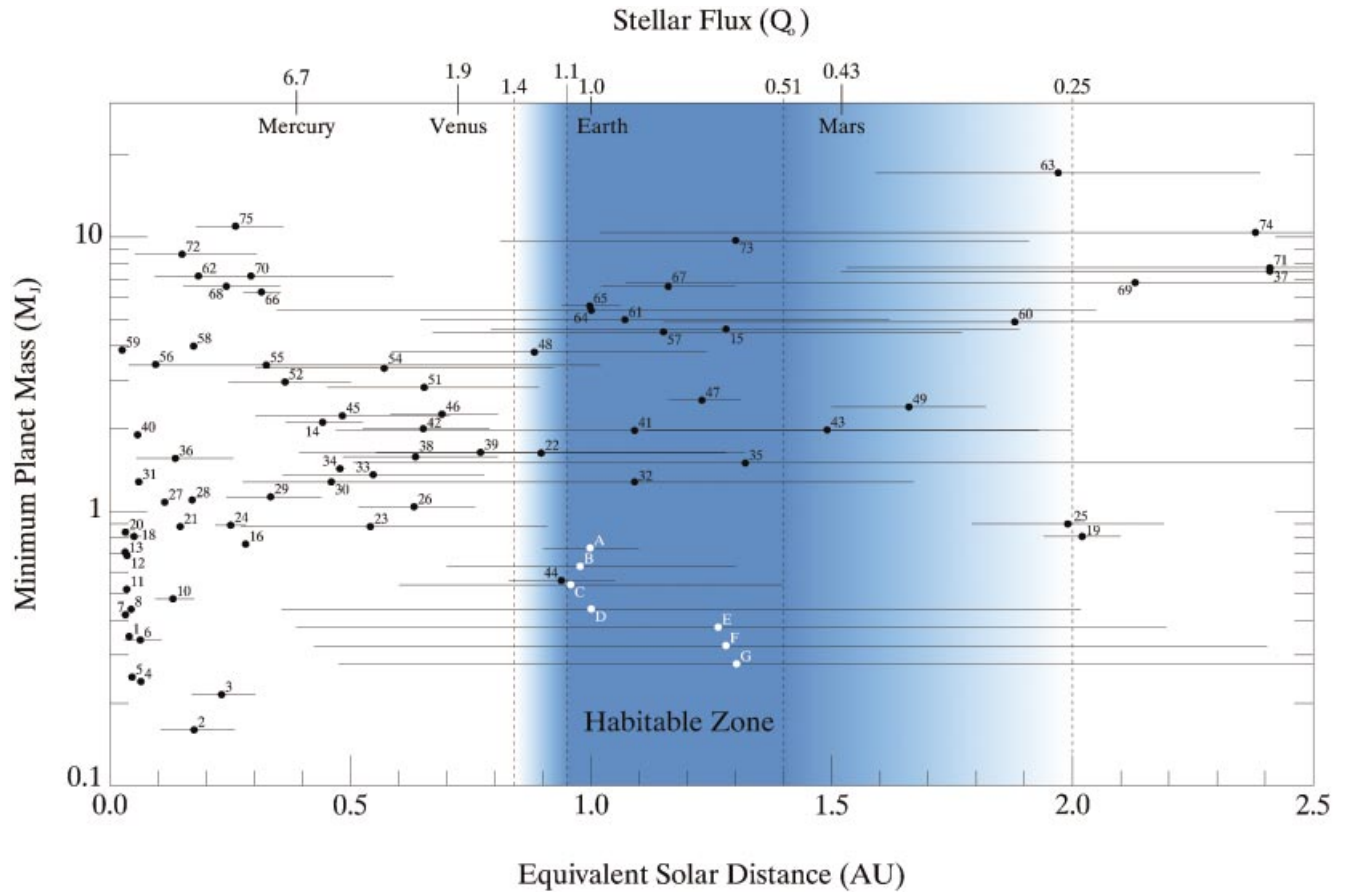
Fig. 1. Locations of the newly discovered extrasolar planets (as of January 2001) relative to the habitable zone around their stars. Equivalent solar distance is the distance a planet would be from the Sun in a circular orbit to receive the same mean orbital flux that it does around its own star. Minimum planet mass relative to the mass of Jupiter is equal to $m \sin i$, where m is the actual planet mass and i is the inclination of the planet's orbit relative to our line sight. Stellar flux is given in units of $Q_0 = 1370$ W m^{-2}, which is the present-day solar constant received by Earth at 1.0 AU from the Sun. The orbital fluxes received by the terrestrial planets around the Sun are shown for comparison at the top of the figure. Habitable zone limits are marked with vertical dashed lines and varying shades of blue. The edges at 0.95 AU ($1.1Q_0$) and 0.84 AU ($1.4Q_0$) denote where Earth would experience a moist stratosphere and runaway greenhouse, respectively. The conservative outer edge at 1.40 AU ($0.51Q_0$) marks where CO_2 clouds would become widespread in a dense CO_2 atmosphere. The non-conservative outer edge at 2.0 AU ($0.25Q_0$) denotes the plausible limit for maximum CO_2 cloud warming. Solid horizontal lines mark the range of orbital distances for planets in eccentric orbits. Locations and range of orbital distances of the planets modelled for this study are shown in white; masses of the seven study planets were chosen arbitrarily for this display.

vapour to condense below the tropopause), and 0.84 AU where the surface temperature climbs dramatically in a positive-feedback loop (higher temperatures → more water vapour → higher temperatures) leading to a runaway greenhouse effect. These are conservative limits because they do not include the cooling effects of clouds of water vapour, which should prevent water loss to slightly greater values of stellar flux. The HZ outer edge is made uncertain by the radiative effects of CO_2 clouds in a CO_2-dominated atmosphere that would form as a result of the negative feedback response of the carbonate–silicate weathering cycle (Williams and Kasting 1997). As a planet surface cools, the rate of silicate weathering by CO_2 dissolved in rain water (carbonic acid) decreases and ultimately stops once the surface freezes. The reduced rate of carbon burial in the crust coupled with an approximately constant rate of CO_2 production by volcanoes causes atmospheric CO_2 levels to rise, which warms the planet surface.

Steady-state CO_2 levels exceeding 1 bar are expected for planets near the HZ outer edge. Given an approximately constant rate of CO_2 outgassing, Kasting *et al.* (1993) and later Williams & Kasting (1997) assumed that CO_2 clouds would act to cool a planet surface by scattering more sunlight than infrared light from the surface. CO_2 clouds began to form in Kasting's one-dimensional (1D) model at 1.37 AU and so he used this distance as the most conservative estimate of the HZ outer edge. Williams and Kasting later used a latitudinally resolved energy-balance model to show that CO_2 clouds first appear over Earth's poles at 1.30 AU and global coverage ensues beyond 1.46 AU. Thus, the problems associated with CO_2 clouds should not become apparent until the clouds become widespread beyond ~ 1.40 AU. Recent work by Forget & Pierrehumbert (1997) and Mischna *et al.* (2000), however, indicates that CO_2 cloud cover could conceivably warm a planet surface by Mie scattering in the infrared

provided the clouds are cold (lofty), cover the entire surface, and have an optical thickness $\tau \sim 10$. Both groups found that under optimal conditions surface temperatures on an Earth-like planet could be maintained above 273 K out to 2.4 AU, but Mischna *et al.* also found significantly less warming under a less-optimized cloud cover.

An important uncertainty here is the CO_2 cloud lifetime, which might be short if the cloud particles snow out on to the surface soon after forming, as occurs on Mars today. The seasonal sequestering of CO_2 at the Martian poles is enough to cause atmospheric pressures to vary in the Martian atmosphere by ~ 3 mbar, which is an important driver of large-scale dust storms (Tillman 1988). CO_2 clouds on a larger planet might not remain aloft long enough to keep the surface above 273 K out to 2.0 AU. In this case the outer edge of the HZ would be 1.40–1.46 AU (Williams & Kasting 1997), where clouds would form temporarily over most of the planet before snowing out on to the ground, thereby causing atmospheric CO_2 levels and surface temperatures to fall. Given the many uncertainties surrounding the nature of CO_2 clouds, we will assume for this discussion that the HZ outer edge around the Sun is ~ 2.0 AU.

The habitable zone limits around the Sun can be used to determine which of the new extrasolar planets are capable of supporting life. The worlds discovered thus far are probably gas-rich objects akin to the planets Jupiter and Saturn, and so are unlikely to harbour life themselves. But any of these substellar objects, even those which turn out to be brown dwarfs, could have solid satellites comparable in size to Mars or even Earth with long-lived atmospheres (Williams *et al.* 1997). Such colossal moons might form through pairwise accretion of small bodies in a proto-satellite disc, as is thought to have happened for the largest moons of Jupiter and Saturn, but only if the disc is massive enough. A more attractive alternative is to form large moons by gas-assisted capture of terrestrial-sized objects in the proto-satellite disks of young giant planets (Williams & Sands 2001), perhaps while the giant planets are migrating inward through the proto-planetary disks surrounding their stars.

An important difference between the planets in the Solar system and those around other stars is orbital eccentricity. The largest orbital eccentricity of any planet in the Solar system is that of Pluto with $e = 0.250$. By comparison, approximately one-third of the newly discovered planets have orbital eccentricities $e > 0.4$, which carries some of the planets and any moons they might possess into and out of the HZ over a single orbit. And although the localized extremes in stellar insolation near periastron and apoastron are damaging to liquid-water environments, such worlds might still be habitable (i.e. avoid a runaway greenhouse or global refrigeration) if they receive a stellar flux that, when averaged over a complete orbit, is not too different from the nearly constant solar flux received by Earth around the Sun (~ 1370 W m^{-2}). In an eccentric orbit, the ratio of periastron to apoastron flux $[\{1+e\}/\{1-e\}]^2$ becomes comparable to the ratio of summer to winter solstice flux at mid-latitude (35°) and present obliquity (23.5°) once eccentricity reaches ~ 0.2. Thus, the

seasonal cycles of moons around extrasolar giant planets (many with $e > 0.4$) will be more strongly affected by the shapes of their orbits than their spin-axis tilts, provided their axial tilts are small. The time-averaged flux over an eccentric orbit is given by the equation

$$\langle F \rangle = \frac{L}{4\pi a^2 (1-e^2)^{1/2}}. \tag{2}$$

Thus, the average orbital flux rises with increasing eccentricity despite the object spending a greater amount of time further from the star than in a circular orbit of radius a.

Fig. 1 shows that 19 of the new extrasolar planets are located within the HZ around their stars. The planets are plotted according to their time-averaged orbital flux, which varies from one planetary system to another because of differences in stellar luminosity (Table 1). Most of the planets within the narrow HZ limits between $0.95 < d' < 1.4$ AU (d' is the 'equivalent solar distance' of Fig. 1) do not remain there over a full orbit. The planet HD 222582 b ($e = 0.71$), for example, spends most of its time well outside the HZ margins, being heated more strongly than Mercury near periastron ($d' = 0.347$ AU) and far less than Mars near apoastron ($d' = 2.05$ AU). Still, moons belonging to planets such as HD 222582 b might be suitable for life if they possess enough volatiles in their oceans or atmospheres to moderate the climatic extremes caused by high eccentricity.

Results

For this study, we used a three-dimensional climate model, GENESIS 2 (Thompson & Pollard 1997; Pollard & Thompson 1995), and a latitudinally resolved energy-balance climate model (Williams & Kasting 1997), or EBM, to simulate how an Earth-like planetary environment would respond to extreme variations in stellar flux in an eccentric orbit. GENESIS 2 is an atmospheric general circulation model coupled to multi-layer surface models of vegetation, soil, land ice and snow, with a diurnal cycle, spectral transform dynamics for mass, heat and momentum, and semi-Lagrangian transport of water vapour. Sea-surface temperatures and sea ice are calculated using a 50 m thermodynamic slab and dynamic sea ice model. The atmospheric grid is spectral T31 ($\sim 3.75°$) with 18 vertical levels, and the grid for all surface models is $2° \times 2°$. The semi-major axis a and orbital period P were set to 1.0 AU and 365 days, respectively, for all of our model runs and solar luminosity was varied to simulate climates at different locations within the HZ. For simplicity, we also fixed the tilt of the spin axis, continental topography and atmospheric composition to resemble our own planet, while recognizing that worlds around other stars are likely to be very different from Earth. The date of vernal equinox was also fixed in our runs to be March 21. Periastron precedes vernal equinox by an orbital longitude = 77°, the same as for present Earth. The time between periastron and vernal equinox is a variable quantity, however, because orbital speed depends on orbital longitude as well as eccentricity. Thus the periastron dates for

Table 1. *Known parameters for the new extrasolar planets and their parent stars*

Spectral type, V_{mag}, and parallaxes for the stars were obtained from the web-based Hipparcos catalogue on the internet (see references). The bolometric corrections (BC) of the stars were approximated using their spectral types and data listed in tables A13 and A14 in Carroll & Ostlie (1996). Stellar distances and luminosities were calculated using the above data and procedures described in the text. Planetary parameters were obtained from data posted on the web-based Extrasolar Planets catalogue (see references) and maintained by Jean Schneider.

No.	Object	Spectral type	V_{mag}	BC	m_{bol}	Parallax (mas)	Distance (pc)	Luminosity ($L_\odot$)	a (AU)	e	$m\sin i$
1	HD 83443 b	K0 V	8.3753	−0.31	8.0653	22.97	43.54	0.90	0.038	0.08	0.35
2	HD 83443 c	K0 V	8.3753	−0.31	8.0653	22.97	43.54	0.90	0.174	0.42	0.17
3	HD 16141 b	G5 IV	6.9642	−0.28	6.6842	27.85	35.91	2.18	0.35	0.28	0.215
4	HD 168746 b	G5	8.0882	−0.21	7.8782	23.19	43.12	1.05	0.066	0	0.24
5	HD 46375 b	K1 IV	8.0512	−0.42	7.6312	29.93	33.41	0.79	0.041	0.04	0.249
6	HD 108147 b	F8/G0 V	7.1120	−0.17	6.9420	25.93	38.57	1.99	0.098	0.558	0.34
7	HD 75289 b	G0 V	6.4749	−0.18	6.2949	34.55	28.94	2.03	0.046	0.053	0.42
8	51 Pegasi b	G5 V	5.5865	−0.21	5.3765	65.10	15.36	1.33	0.0512	0.013	0.44
9	BD-103166 b	G4 V	–	−0.20	–	–	–	–	0.046	0.05	0.48
10	HD 6434 b	G3 IV	7.8495	−0.30	7.5495	24.80	40.32	1.24	0.15	0.3	0.48
11	HD 187123 b	G5	7.9689	−0.21	7.7589	20.87	47.92	1.45	0.042	0.03	0.52
12	HD 209458	F8	7.7719	−0.16	7.6119	21.24	47.08	1.60	0.045	0	0.69
13	Upsilon And b	F8 V	4.2118	−0.16	4.0518	74.25	13.47	3.47	0.059	0.034	0.71
14	Upsilon And c	F8 V	4.2118	−0.16	4.0518	74.25	13.47	3.47	0.83	0.18	2.11
15	Upsilon And d	F8 V	4.2118	−0.16	4.0518	74.25	13.47	3.47	2.5	0.41	4.61
16	HD 192263 b	K0	7.9310	−0.31	7.6210	50.27	19.89	0.28	0.15	0.03	0.75
17	Epsilon Eridani	K2 V	3.8652	−0.42	3.4452	310.75	3.22	0.35	3.3	0.608	0.86
18	HD 38529 b	G4	6.0802	−0.20	5.8802	23.57	42.43	6.40	0.1293	0.27	0.77
19	HD 4208 b	GS V	7.923	−0.21	7.7130	30.58	32.70	0.70	1.69	0.04	0.81
20	HD 179949 b	F8 V	6.3620	−0.16	6.2020	36.97	27.05	1.93	0.045	0.05	0.84
21	55 Cancri b	G8 V	6.1054	−0.40	5.7054	79.80	12.53	0.66	0.1183	0.03	0.88
22	HD 82943 b	G0	6.6686	−0.18	6.4886	36.42	27.46	1.53	1.16	0.41	1.63
23	HD 82943 c	G0	6.6686	−0.18	6.4886	36.42	27.46	1.53	0.73	0.54	0.88
24	HD 121504 b	G2 V	7.6706	−0.20	7.4706	22.54	44.37	1.62	0.32	0.13	0.89
25	HD 114783 b	K0	7.7194	−0.31	7.4094	48.95	20.43	0.36	1.2	0.1	0.9
26	HD 37124 b	G4 IV-V	7.7918	−0.24	7.5518	30.08	33.24	0.84	0.585	0.19	1.04
27	HD 130322 b	K0 III	8.1843	−0.50	7.6843	33.60	29.76	0.60	0.088	0.048	1.08
28	Rho CrB b	G2 V	5.5246	−0.20	5.3246	57.38	17.43	1.80	0.23	0.028	1.1
29	HD 52265 b	G0 III-IV	6.4132	−0.20	6.2132	35.63	28.07	2.06	0.49	0.29	1.13
30	HD 177830 b	K0	7.3455	−0.31	7.0355	16.94	59.03	4.27	1.00	0.43	1.28
31	HD 217107 b	G8 IV	6.3124	−0.40	5.9124	50.71	19.72	1.34	0.07	0.14	1.28
32	HD 210277 b	G0	6.6823	−0.18	6.5023	46.97	21.29	0.91	1.097	0.45	1.28
33	HD 142	G1 IV	5.8163	−0.20	5.6163	39.00	25.84	2.98	0.98	0.37	1.36
34	HD 27442 b	K2 IVa	4.5977	−0.50	4.0977	54.84	18.23	6.10	1.18	0.02	1.43
35	16 Cygni Bb	G5 V	6.3656	−0.21	6.1556	46.70	21.41	1.26	1.72	0.67	1.5
36	HD 74156 b	G0	7.7415	−0.18	7.5615	15.49	64.56	3.15	0.276	0.649	1.56
37	HD 74156 c	G0	7.7415	−0.18	7.5615	15.49	64.56	3.15	3.47	0.395	7.5
38	HD 134987 b	G5 V	6.6023	−0.21	6.3923	38.98	25.65	1.46	0.78	0.24	1.58
39	HD 4203 b	G5	8.8454	−0.21	8.6354	12.85	77.82	1.70	1.09	0.53	1.64
40	HD 68988 b	G0	8.3356	−0.18	8.1556	17.00	58.82	1.51	0.071	0.14	1.9
41	HD 160691 b	G5 V	5.2585	−0.21	5.0485	65.46	15.28	1.78	1.65	0.62	1.97
42	HD 19994 b	F8 V	5.1852	−0.16	5.0252	44.69	22.38	3.91	1.3	0.2	2.0
43	Gliese 876 b	M5	10.1480	−2.73	7.4180	212.69	4.70	0.02	0.21	0.1	1.89
44	Gliese 876 c	M5	10.1480	−2.73	7.4180	212.69	4.70	0.02	0.13	0.27	0.56
45	HD 8574 b	F8	7.2497	−0.16	7.0897	22.65	44.15	2.27	0.76	0.4	2.23
46	HR 810 b	G3 IV	5.5181	−0.25	5.2681	58.00	17.24	1.86	0.925	0.161	2.26
47	HD 23079 b	G0 V	7.2389	−0.18	7.0589	28.90	34.60	1.44	1.48	0.06	2.54
48	HD 92788 b	G5	7.4518	−0.21	7.2418	30.94	32.32	1.06	0.95	0.3	3.83
49	47 UMa b	G0 V	5.1572	−0.18	4.9772	71.04	14.08	1.62	2.11	0.096	2.4
50	47 UMa c	G0 V	5.1572	−0.16	4.9772	71.04	14.08	1.62	3.73	0.1	0.76
51	HD 12661 b	K0	7.5670	−0.31	7.2570	26.91	37.16	1.38	0.8267	0.328	2.8
52	HD 169830 b	F8 V	6.0109	−0.16	5.8509	27.53	36.32	4.82	0.823	0.34	2.96
53	14 Her b	K0 V	6.7595	−0.31	6.4495	55.11	18.15	0.69	2.5	0.326	3.3
54	GJ 30216	G6 V	6.7233	−0.25	6.4733	56.76	17.62	0.64	0.49	0.505	3.32
55	HD 80606 b	G5	9.2087	−0.21	8.9987	17.13	58.38	0.69	0.439	0.927	3.41
56	HD 195019 b	G3 IV-V	7.0103	−0.23	6.7803	26.77	37.36	2.16	0.14	0.05	3.43
57	HD 213240 b	G4 IV	6.9407	−0.24	6.7007	24.54	40.75	2.77	1.6	0.31	3.7
58	Gliese 86 b	K0 V	6.2571	−0.31	5.9471	91.63	10.91	0.40	0.11	0.046	4.0

Table 1 (*cont.*)

| No.	Object	Spectral type	V_{mag}	BC	m_{bol}	Parallax (mas)	Distance (pc)	Luminosity ($L_\odot$)	a (AU)	e	$m \sin i$
59	Tau Boo b	F7 V	4.5949	−0.16	4.4349	64.12	15.60	3.27	0.0475	0	4.09
60	HD 50554 b	F8	6.9706	−0.16	6.8106	32.23	31.03	1.45	2.38	0.42	4.9
61	HD 190228 b	G5 IV	7.4520	−0.28	7.1720	16.10	62.11	4.17	2.31	0.43	4.99
62	HD 168443 b	G5	7.0638	−0.21	6.8538	26.40	37.88	2.08	0.29	0.55	7.2
63	HD 168443 c	G5	7.0638	−0.21	6.8538	26.40	37.88	2.08	2.87	0.2	17.1
64	HD 222582 b	G5	7.8188	−0.21	7.6088	23.84	41.95	1.27	1.35	0.71	5.4
65	HD 28185 b	G5	7.9484	−0.21	7.7384	25.28	39.56	1.00	1	0.06	5.6
66	HD 178911 Bb	G5	8.2885	−0.21	8.0785	21.40	46.73	1.02	0.439	0.145	6.47
67	HD 10697 b	G5 IV	6.4169	−0.28	6.1369	30.71	32.56	2.97	2	0.12	6.59
68	70 Vir b	G5 V	5.1033	−0.21	4.8933	55.22	18.11	2.89	0.43	0.4	6.6
69	HD 106252 b	G0	7.5473	−0.18	7.3673	26.71	37.44	1.27	2.61	0.54	6.81
70	HD 89744 b	F7 V	5.8479	−0.16	5.6879	25.65	38.99	6.45	0.88	0.7	7.2
71	HD 33636 b	G0	7.1300	−0.18	6.9500	34.85	28.69	1.09	2.62	0.39	7.71
72	HIP 75458 b	K2 III	3.4638	−0.60	2.8638	31.92	31.33	58.12	1.34	0.71	8.64
73	HD 141937 b	G2-3 V	7.3824	−0.20	7.1824	29.89	33.46	1.20	1.49	0.404	9.7
74	HD 39091 b	G3 IV	5.7855	−0.20	5.6855	54.92	18.21	1.55	3.34	0.62	10.37
75	HD 114762 b	F9 V	7.4130	−0.19	7.2230	24.65	40.57	1.70	0.351	0.335	10.93

+, formerly Iota Hor b.
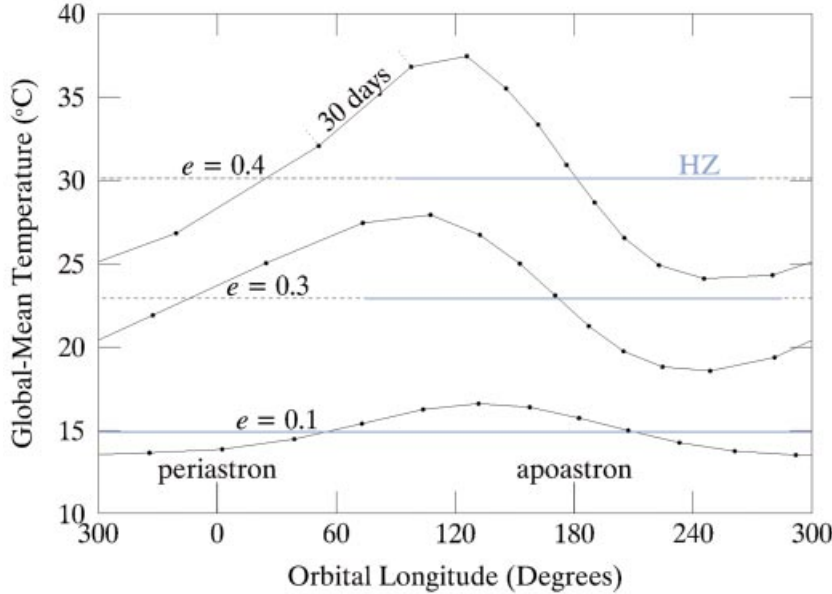
Fig. 2. Orbital variation of global mean temperature for the study planets of GCM runs 1–3 with orbital eccentricities of 0.1, 0.3 and 0.4, respectively. Seasonal mean temperatures are indicated by horizontal dashed lines partially covered by thick blue lines to mark the range of orbital longitudes for which each planet is within the HZ. Orbital longitude, or *true anomaly*, is 0° at periastron when the planet is closest to its star and 180° at apoastron when the planet is furthest away. The black points denote actual model data spaced 1 month (∼ 30 days) apart.

GCM runs 1–4 with eccentricities $e = 0.1, 0.3, 0.4$ and 0.7 are January 13, February 2, 11 and March 7, respectively.

For the first set of runs (GCM runs 1–3), we examined how an Earth-like planet would respond to increasing the eccentricity of its orbit near the inner edge of the HZ while holding solar luminosity, orbital semi-major axis, and pCO_2 (345 ppmv) constant. The range of orbital distances is shown for each of the runs in Fig. 1, and the results of the runs are given in Fig. 2 and Table 2. Increasing eccentricity from Earth's present value of 0.0167 to 0.4 causes the seasonal-global mean surface temperature to increase from 14.6 °C at present to 30.1 °C. The time spent within the HZ also decreases

from 365 days for $e \leqslant 0.1$ to approximately 180 days for $e = 0.4$. The detailed climate results (not shown here) reveal that relative humidity and precipitation rise significantly with increasing temperature, particularly near periastron when the seasonal cycle owing to eccentricity reaches its peak.

The rise in relative humidity at high temperatures results directly from an increased rate of evaporation of water from the oceans, and is the first stage of climate destabilization by the moistening of the lower atmosphere and later the stratosphere where water can be readily lost through photo-dissociation of water vapour. However, the steep temperature gradient in the lower atmosphere effectively prevents moisture

Table 2. *Model input and output for the climate runs*

GCM indicates that the run was performed using the general-circulation climate model (GENESIS II) developed by Thompson & Pollard (1997), and EBM refers to the energy-balance model of Williams & Kasting (1997). Letters used to label the planets in Figure 1 are given in column 2. Orbital semi-major axis and orbital period were 1.0 AU and 365 days for each run. Obliquity (23.45°), continental topography and concentrations of primary gases (with the exception of H_2O and CO_2) in Earth's atmosphere were also maintained at present values. Carbon dioxide levels for GCM runs 1–4 and EBM run 1 were held fixed at 345 ppmv, whereas the levels reported for EBM runs 2–5 were calculated using the model by accounting for the effects of carbonate–silicate weathering.

Runs	Fig 1	Eccentricity	Luminosity $(L_\odot)$	pCO_2 (bars)	T_{ave} (°C)
GCM 1	A	0.1	1.00	3.45×10^{-3}	14.90
GCM 2	B	0.3	1.00	3.45×10^{-3}	22.90
GCM 3	C	0.4	1.00	3.45×10^{-3}	30.11
GCM 4	D	0.7	0.71	3.45×10^{-3}	22.45
EBM 1	D	0.7	0.71	3.45×10^{-3}	21.17
EBM 2	D	0.7	0.71	4.28×10^{-4}	12.94
EBM 3	E	0.7	0.60	5.03×10^{-2}	14.82
EBM 4	F	0.7	0.50	3.39×10^{-1}	16.17
EBM 5	G	0.7	0.40	1.28×10^{0}	17.03

from reaching the stratosphere until global-mean surface temperatures exceed $\sim 65\,°C$ (Kasting *et al.* 1993). Although localized temperatures for GCM run 3 with $e = 0.4$ exceed $70\,°C$ near the peak of the seasonal cycle, the seasonal- and global-mean surface temperatures for all of the study planets are well below the temperatures needed to efficiently deliver moisture to the stratosphere. Setting stellar flux defining the HZ inner edge ($1.1Q_0$ or $1.4Q_0$ – see Fig. 1) equal to the average flux received by a planet in an eccentric orbit (equation 2), yields an upper limit on orbital eccentricity for planets at 1.0 AU to hold their water around a star with a luminosity of $1.0\,L_\odot$. The eccentricity limit for preventing water from reaching the stratosphere is 0.42 and the limit associated with a runaway greenhouse is 0.70. Both limits would place the planet well outside the HZ near periastron in the same region of space occupied by Mercury and Venus in the Solar system.

Planets with orbital eccentricities of ~ 0.7 and higher have recently been discovered around nearby stars. Noteworthy examples are 16 Cygni Bb ($e = 0.67$), HD 222582 b ($e = 0.71$) and HD 80606 b ($e = 0.927!$). Such orbits are thought to result from close interplanetary encounters or collisions during the late stages of accretion in proto-planetary disks and may represent the end-state of dynamically unstable systems (Rasio & Ford 1996). Fig. 1 shows that 16 Cygni Bb and HD 222582 b receive mean orbital fluxes that place them within the limits of the HZ and, thus, could have Earth-like moons capable of supporting life. Fig. 1 also shows that both worlds spend only a fraction of their orbits within the HZ.

Our final GCM run was performed to simulate the climate of such a world with an orbital eccentricity of 0.7. For this run, the orbital semi-major axis was maintained at 1.0 AU and solar luminosity was scaled by 0.714 to give the planet the same mean orbital flux as Earth would receive in a circular orbit. This adjustment to the solar luminosity was made to

model more closely the mean orbital flux received by 16 Cygni Bb and HD 222582 b at their respective distances from their stars, and to ensure that the seasonal-global mean temperature for our simulated planet was not too different from present Earth. The range of distances and fluxes for GCM run 4 is shown in Fig. 1.

The GCM output parameters for run 4 were calculated every 5 days to obtain a more precise picture of how climate responds to the rapidly varying stellar flux near periastron. Thus, 73 frames of output were written over a complete 365 day orbit. Global temperature maps for three different orbital longitudes ($104° =$ warmest, $180° =$ apoastron, $220° =$ coldest) are shown in Fig. 3. The seasonal cycle for global mean temperature is shown in Fig. 4, which indicates that our simulated planet is $\sim 7.8\,°C$ warmer on average than present Earth even though it receives the same mean-orbital stellar flux. The higher model temperature results from a reduction in seasonal albedo due to reductions in the amounts of snow and ice cover over the continents and polar oceans. Other climate indicators for this run that differ significantly from present Earth are precipitation and horizontal wind speed which increase twofold over oceanic (high precipitation) and continental (windy) areas, respectively, in our super-heated model atmosphere.

The hottest surface temperatures of our planet occur at an orbital longitude of $104°$ (see Fig. 3a), when surface temperatures exceed $80\,°C$ over a large portion of the continents. Although these warm temperatures would be damaging to many forms of life on Earth today, the planet studied spends only 60–90 days in this super-heated state as a consequence of its high orbital speed near periastron. Our planet actually spends most ($\sim 64\%$) of its time beyond the outer edge of the HZ, reaching equivalent solar distances of 2.02 AU ($= 1.7$ AU around the Sun) where it is able to cool to temperatures well below those in Fig. 3a, but still remain above freezing. Fig. 4 demonstrates that the planet passes through the HZ twice over an orbit. The 'warm' HZ passage, with global-mean temperatures $> 35\,°C$, occurs less than 1 month after periastron at an orbital longitude $\sim 120°$, while the second 'cold' passage, with temperatures $\sim 11\,°C$ (Fig. 3c), commences at an orbital longitude of $\sim 210°$. The 50 m mixed ocean layer in the GCM provides enough thermal inertia to maintain liquid water all year round, even though less than 75 days is spent within the HZ. Although the neglect of ocean dynamics and deep thermohaline circulations probably affects some regional details of our results, the basic aspects are very likely to be robust.

In addition, the damaging high- and low-temperature extremes in a highly eccentric orbit should be damped on planets that exhibit climate-buffering carbonate–silicate weathering cycles, which control the amount of CO_2 that resides in the atmosphere. In this cycle the efficiency of carbon burial in the crust is temperature dependent, which causes the atmospheric CO_2 level to increase (decrease) over geological time-scales when surface temperatures fall (rise). Thus, Earth-like planets in either circular or eccentric orbits near the outer edge of the HZ are expected to develop dense CO_2
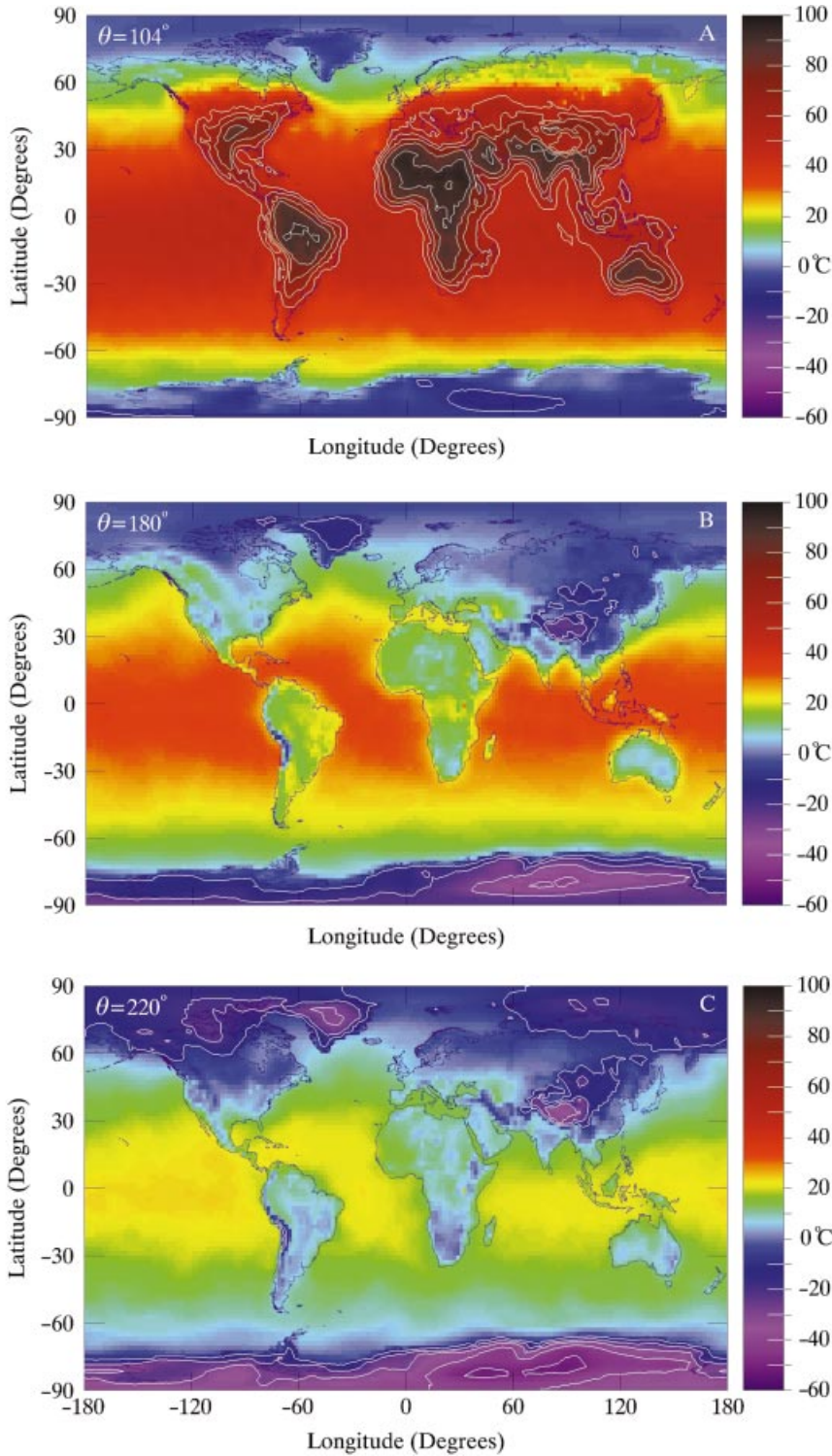
Fig. 3. Representative temperature maps for the study planet of GCM run 4. White contours spaced every 10 °C mark temperatures $\geqslant 50$ °C and $\leqslant -10$ °C. The three maps A–C show temperatures for a planet on an extremely eccentric orbit ($e = 0.7$) at orbital longitudes of $\theta = 104°$, $180°$ (apoastron) and $220°$, respectively. While extreme continental temperatures > 80 °C in frame A suggest that such a planet might not be suitable for water-dependent life, the planet spends less than 60 days in this superheated state as it moves rapidly by the star near periastron. The maps in frames B and C are more representative of temperatures over the remainder of the orbit when the planet's orbital longitude is changing more slowly.

atmospheres, which store and transport heat much more efficiently than Earth's atmosphere (Williams & Kasting 1997).

We performed a final series of climate runs using the EBM of Williams & Kasting to model the climate of planets on eccentric orbits with the carbonate–silicate weathering feedback included. EBM run 1 was performed with the same
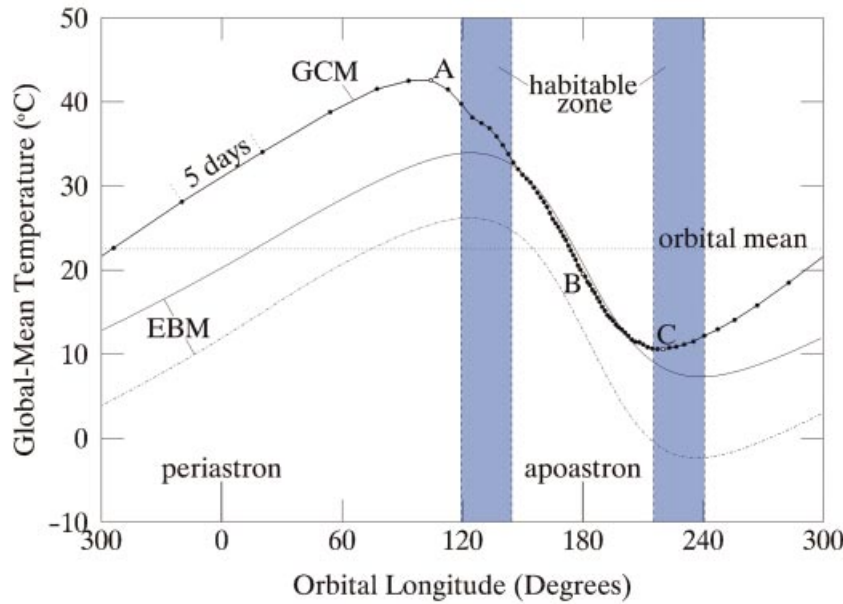
Fig. 4. Orbital variation of global mean temperature for the study planets of GCM run 4, and EBM runs 1 and 2. Black points denote actual model data for GCM run 4 spaced evenly in time by 5 days and the white points labelled A–C refer to the three temperature maps shown in Fig. 3. Orbital longitude is the orbital *true anomaly*, or the angle between the planet direction and periastron when viewed from the orbit focus. Habitable zone boundaries correspond to orbital longitudes (or distances) at which the flux is equal to that received by a planet at distances of 0.9 and 1.4 AU around the Sun. The orbital mean temperature for GCM run 4 is 22.45 °C, approximately 7 °C warmer than Earth today despite the planet spending nearly two-thirds of the 365 day orbit well beyond the outer edge of the habitable zone near apoastron. Periastron and apoastron distances are 0.3 and 1.7 AU, respectively. Seasonal cycles for the study planets of EBM runs 1 and 2 are shown as a thin solid line and thin broken line respectively. The large differences between the GCM and EBM results are mainly due to the poorer resolution of the EBM, which fails to accurately model the high temperatures over continental interiors following periastron.

orbital and stellar parameters as GCM run 4, and with pCO_2 held fixed at 345 ppmv, the same value used in GCM runs 1–4 (Table 2). This was done to enable a direct comparison of the EBM and GCM results for the same initial atmospheric parameters. The results in Table 2 and Fig. 4 show that the planet simulated by the EBM with fixed CO_2 (thin solid line) is slightly (~ 1.5 °C) colder on average than the planet simulated by the GCM (thick solid line). In addition, the seasonal cycle for EBM run 1 lags the GCM run 4 cycle by $\theta \sim 30°$. Both of these differences may be attributed to the higher zonally averaged heat capacity used in the EBM (equivalent to a 50 m column of water), which yields a slower rate of seasonal warming and cooling and a smaller amplitude for the seasonal cycle. Despite these minor dissimilarities, the model results are in close enough agreement to lend credence to the other EBM results described below.

For EBM run 2, the model was allowed to calculate the steady-state CO_2 level required to balance the rate of CO_2 production by volcanoes with the rate of weathering and carbon burial for a particular seasonal temperature cycle. The small increase in the seasonal-global mean temperature for GCM run 4 and EBM run 1 with $e = 0.7$ and $L = 0.71 L_\odot$ causes pCO_2 to decrease from 345 to 42.8 ppmv (Table 1) in EBM run 2. This is mainly a result of the increased rate of weathering over the warm continents (Fig. 3a) near periastron. Weathering of extremely hot (and possibly dry) continental surfaces may be far less efficient than weathering that occurs on the warm areas of Earth today. The planet

cools slightly from 21.2 to 12.9 °C (Table 2) as a result of the decrease in pCO_2, which is indicated by a lowering of the seasonal temperature cycle (dashed line) in Fig. 4.

We also used the EBM to calculate equilibrium CO_2 levels for planets further out in the HZ by reducing the solar luminosity from 0.71 $L_\odot$ to 0.6, 0.5 and 0.4 $L_\odot$ while keeping e and a constant. The range of orbital distances and stellar fluxes are shown in Fig. 1 and the run results are listed in Table 1. The resulting trend is for the steady-state CO_2 to increase to counteract the decrease in solar luminosity. This is because the weathering rate slows when a planet becomes cold, which allows CO_2 to accumulate in the atmosphere given an approximately constant rate of CO_2 outgassing through volcanoes. The CO_2 level for EBM runs 3–5 is shown to increase from 0.05 bars to 1.28 bars as the scaled semi-major axis a' increases from 1.09 to 1.33 AU, in close agreement with the CO_2 levels calcuated by Williams & Kasting (1997) for planets in circular orbits. The rise in pCO_2 as the planet is moved toward the outer edge of the HZ causes the seasonal-global mean temperature to *increase* from 12.9 to 17.0 °C, which is warmer than Earth at 1.0 AU from the Sun. However, such an atmosphere may be unable to keep an Earth-like environment warm under low stellar flux once CO_2 clouds begin to form. The EBM model shows that CO_2 clouds begin to form seasonally at $L = 0.4 L_\odot$, and clouds are expected to become more widespread and possibly problematic once L drops below $\sim 0.35 L_\odot$. Still, the extremes in equivalent solar distance in such an orbit are remarkable for a habitable planetary en-

vironment; for $L = 0.4\ L_{\odot}$ and $e = 0.7$, the planet dips inward to an equivalent solar distance of 0.40 AU at periastron and reaches 2.26 AU at apoastron. This demonstrates that dramatic seasonal changes in stellar flux received over an orbit of moderate-to-high eccentricity do not critically compromise planetary habitability and, thus, serves to expand the arena of possibilities for finding life beyond the Solar system.

References

Carroll, B.W. & Ostlie, D.A. (1996). *An Introduction to Modern Astrophysics*. Addison-Wesley, New York.

Extrasolar Planets catalog (www.obspm.fr/encycl/catalog.html) maintained by Jean Schneider.

Forget, F. & Pierrehumbert, R.T. (1997). *Science* **278**, 1273.

Hipparcos catalog (archive.ast.cam.ac.uk/hipp/hipparcos.html).

Kasting, J.F., Whitmire, D.P. & Reynolds, R.T. (1993). *Icarus* **101**, 108.

Mischna, M.A., Kasting, J.F., Pavlov, A. & Freedman, R. (2000). *Icarus* **145**, 546.

Pollard, D. & Thompson, S.L. (1995). *Glob. Planet Change* **10**, 129.

Rasio, F.A. & Ford, E.B. (1996). *Science* **274**, 954.

Thompson, S.L. & Pollard, D. (1997). *J. Climate* **10**, 871.

Tillman, J.E. (1988). *J. Geophys. Res.* **84**, 2947.

Williams, D.M. & Kasting, J.F. (1997). *Icarus* **129**, 254.

Williams, D.M., Kasting, J.F. & Wade, R.A. (1997). *Nature* **385**, 234.

Williams, D.M. & Sands, B.L. (2001). Gas-assisted capture of Earth-sized moons around extrasolar giant planets. *Bull. Am. Astron. Soc.* **33** (3).

See shahrazad.bd.psu.edu/Williams/ija2002/maps.html for animated temperature maps.